Electron-phonon deformation potential interaction in core-shell Ge-Si and Si-Ge nanowires

Darío G. Santiago-Pérez,[1,2,*] C. Trallero-Giner,[3,4] R. Pérez-Álvarez,[5] Leonor Chico,[6] and G. E. Marques[4]
[1]*Universidad de Sancti Spiritus "José Martí Pérez," Ave. de los Mártires 360, CP 62100, Sancti Spiritus, Cuba*
[2]*CLAF–Centro Latino-Americano de Física, Avenida Venceslau Braz, 71, Fundos 22290-140, Rio de Janeiro, RJ, Brazil*
[3]*Department of Theoretical Physics, Havana University, Havana 10400, Cuba*
[4]*Departamento de Física, Universidade Federal de São Carlos, 13.565-905 São Carlos, Brazil*
[5]*Universidad Autónoma del Estado de Morelos, Ave. Universidad 1001, CP 62209, Cuernavaca, Morelos, Mexico*
[6]*Instituto de Ciencia de Materiales de Madrid (ICMM), Consejo Superior de Investigaciones Científicas (CSIC), C/Sor Juana Inés de la Cruz 3, 28049 Madrid, Spain*

(Received 30 September 2014; revised manuscript received 30 December 2014; published 24 February 2015)

We settle a general expression for the Hamiltonian of the electron-zone-center optical phonon deformation potential (DP) interaction in the case of nonpolar core-shell cylindrical nanowires (NWs). On the basis of a long-range phenomenological continuum model for the optical modes and by taking into account the bulk phonon dispersions, we study the size dependence and strain-induced shift on the electron-phonon coupling strengths for Ge-Si and Si-Ge NWs. We derive analytically the DP electron-phonon Hamiltonian and report some numerical results for the frequency core modes and vibrational amplitudes. Our approach allows for the unambiguous identification of the strain and confinement effects on the optical phonons at the Γ point. We explore the dependence of mode frequencies, phonon amplitudes, and hole-DP scattering rate on the spatial symmetry and the structural parameters of these core-shell structures, which constitute a basic tool for the characterization and device applications of these novel nanosystems.

DOI: 10.1103/PhysRevB.91.075312 PACS number(s): 63.20.kd, 63.20.D−, 63.22.Gh

I. INTRODUCTION

Semiconductor nanowires are at the focus of intense research due to their potential design of nanoscale devices, with applications in electronics, photonics, and nanosensors; in addition, they constitute unique systems to explore novel low-dimensional phenomena, with great basic interest [1–3]. The experimental progress on the fabrication of core-shell nanowires has expanded the possibilities for tailoring the physical properties of these structures. Systems composed by Si, Ge, and their solid solutions, are among the most studied and emerging as natural choices for integration with Si-based electronics. The successful synthesis of Si-Ge core-shell nanowires [4] and the variety of applications foreseen for these materials have boosted the interest of many researchers [5–14]. Distinct physical properties, such as the separation of electron and hole carriers or the dramatic reduction of the thermal conductivity, are attained in Ge-Si core-shell nanowires (NWs). Furthermore, with this cylindrical geometry it is possible to achieve much higher strains between the two materials without losing crystalline coherence [15], which can be of interest to modify the carrier mobility and effective masses in these nanostructures. However, there are limits to the wire diameters that can be grown without yielding defects, such as dislocations at the interface and shell corrugation, in order to relax the stress [16]. The crystalline orientation of the nanowire is another parameter to be considered. In fact, the study of acoustic phonons in strained Si-Ge nanowires has been recently addressed by means of a phenomenological continuum model [17]. Strain may affect the lifetimes of spin qubits in gate-defined quantum dots in semiconductor nanowires and it has important consequences on the electronic and optical properties, not only due to the rehybridization of the electronic bands [18], but also because of induced changes in the spin relaxation lifetime due to spin-phonon coupling [19].

In order to characterize core-shell nanowires, Raman spectroscopy, a nondestructive technique, as well as infrared polarizability (IRP) are widely used to provide information on the phonon response region, the differences between various confined optical vibrations, their angular momentum, dependence size and structural effects, and type of semiconductors involved in a structure. In order to elucidate the Raman selection rules, electronic scattering rates, confinement, and the strain effects in these systems, the knowledge of the electron-phonon Hamiltonian (EPH) as well as the zone-center optical modes of the nanostructure are necessary. By employing a continuum model, we aim at a description of EPH and the dependence of the optical modes on wire radii and phonon symmetry for nonpolar materials.

It is well known (see Ref. [20], and references therein) that in III-V and II-VI semiconductor nanostructures, the Fröhlich-like long-range electrostatic potential is the most relevant interaction. Since Si-Ge and Ge-Si are nonpolar materials, the electrostatic contribution due to the anion-cation atomic vibrations is absent. Consequently, the dominant contribution to the EPH is the mechanical deformation potential (DP) [21]. In this sense, for a reliable description of the interaction between nonpolar vibrations and electronic quasiparticles, it is necessary to have knowledge of phonon displacement vectors and their spatial symmetries. For the particular case of the electron-optical phonon Hamiltonian at the Γ point, these characteristics determine other physical properties, such as hole scattering, transport, Raman efficiency, IRP, and Raman selection rules. Hence, a straightforward explicit expression for the EPH, as well as the understanding of its physical

*Permanent address: U. Sancti Spiritus, Cuba. dariog@cbpf.br, dario@uniss.edu.cu

relevance, represent a central issue for the investigation of these novel structures.

In this work we study the zone-center optical modes and the corresponding electron-optical phonon deformation potential Hamiltonian of core-shell nanowires based on Si and Ge. We address the frequencies, phonon amplitudes, and symmetry dependence on core modes with respect to the relative dimensions of the system, i.e., core radius, shell thickness, ratio between core and shell radii, and the subsequent stress which builds up at the core-shell interface. We analyze the coupling between modes and the dispersion relations for these structures. We focus on core modes, for which the strain is homogeneous, in contrast to shell modes, which present a radial dependence on strain, thus, making it more difficult to distinguish between the contributions of strain and confinement for characterization purposes [15,22]. To this end, we employ a continuum approach, as has been done for other systems [23–25], including core-shell nanowires of polar semiconductors [26,27]. As in the polar case, both core and shell components develop strain due to the different lattice constant between the two materials. We include this effect in our model, so that frequencies at the center of the Brillouin zone of the bulk material are shifted with respect to the unstrained case. Therefore, a macroscopic treatment of the phonon confinement frequencies and their spatial eigensolutions becomes a powerful tool to tackle the electron-optical phonon Hamiltonian in cylindrical core-shell NWs.

This work is organized as follows: Section II addresses the main formalism used to obtain the optical deformation potential Hamiltonian interaction for cylindrical nanowires. Furthermore, we provide an explicit analytical equation for the hole scattering matrix elements in terms of the 4×4 Luttinger Hamiltonian, deformation potential tensor, and phonon field displacements. Section III presents the details of the phenomenological model. A brief review is given in Sec. III A, showing the equations of motion and the explicit form of the basis set for the solutions. Section III B details for the inclusion of strain effects on the vibrational frequencies of the corresponding bulk materials. In Sec. IV we present analytical results for particular cases of the phonon dispersion relations with higher symmetry, which allows us to evaluate the frequency shifts due to confinement effects and strain, as well as the coupling between vibrational modes. Additionally, numerical results for Ge-Si and Si-Ge nanowires are shown. Section V is devoted to an analysis of the zone-center-phonon symmetry on hole scattering rates due to a deformation potential interaction Hamiltonian in the NWs. Finally, we draw our conclusions in Sec. VI.

II. ELECTRON-OPTICAL PHONON INTERACTION IN CORE-SHELL NANOWIRES

In nonpolar semiconductors, the deformation potential is a short-range interaction [21]. Thus, in the framework of the Born-Oppenheimer linear approximation, the electron-phonon interaction can be written as

$$H_{\text{e-ph}} = \vec{u} \cdot \frac{\partial H}{\partial \vec{u}}. \tag{1}$$

Here, $\vec{u}$ is the phonon field displacement and $\partial H/\partial \vec{u}$ takes into account the perturbation of the electronic Hamiltonian by the optical phonon modes at the center of the Brillouin zone.

At the Γ point of the Brillouin zone, the matrix elements between s-like conduction band states is zero and, in consequence, there is no deformation potential interaction between electrons in the conduction band and optical phonons. For the p-like valence band, the $\vec{D} = \partial H/\partial \vec{u}$ components in cylindrical coordinates can be expressed, in matrix representation, as follows (see Appendix A):

$$D_{\hat{e}_r} = \frac{du_0}{a_0}\begin{pmatrix} 0 & -e^{i\theta} & 0 & 0 \\ -e^{-i\theta} & 0 & 0 & 0 \\ 0 & 0 & 0 & e^{i\theta} \\ 0 & 0 & e^{-i\theta} & 0 \end{pmatrix}, \tag{2}$$

$$D_{\hat{e}_\theta} = \frac{idu_0}{a_0}\begin{pmatrix} 0 & -e^{i\theta} & 0 & 0 \\ e^{-i\theta} & 0 & 0 & 0 \\ 0 & 0 & 0 & e^{i\theta} \\ 0 & 0 & -e^{-i\theta} & 0 \end{pmatrix}, \tag{3}$$

and

$$D_{\hat{e}_z} = \frac{idu_0}{a_0}\begin{pmatrix} 0 & 0 & -1 & 0 \\ 0 & 0 & 0 & -1 \\ 1 & 0 & 0 & 0 \\ 0 & 1 & 0 & 0 \end{pmatrix}, \tag{4}$$

with d being the optical DP constant as defined by Bir and Pikus [21], a_0 the lattice constant, $u_0 = (\hbar V_c/VM\omega_0)^{1/2}$ the unit of phonon displacement, V_c the volume of the primitive cell, M the atomic mass, V the volume of the nanowire, and ω_0 the bulk optical phonon frequency at the Γ point. The Hamiltonian for the electron-phonon interaction in the occupation number representation can be expressed as [28]

$$H_{\text{e-ph}} = \sum_{\alpha_h', \alpha_h, j, k_z} M^{(j)}_{\alpha_h', \alpha_h} [a_j^\dagger(k_z) + a_j(-k_z)] c^\dagger_{\alpha_h'} c_{\alpha_h}, \tag{5}$$

where $a_j(k_z)^\dagger [a_j(-k_z)]$ and $c^\dagger_{\alpha_h'}$ (c_{α_h}) denote the phonon and electron creation (annihilation) operators in the j branch with wave vector k_z $(-k_z)$ and state α_h' (α_h), respectively. In Eq. (5), $M^{(j)}_{\alpha_h', \alpha_h}$ represents the amplitude probability of scattering between the electronic states $\alpha_h \to \alpha_h'$ due to the interaction with an optical phonon with a vector displacement $\vec{u}^{(j)}$. This probability amplitude is given by [29]

$$M^{(j)}_{\alpha_h', \alpha_h} = \frac{1}{\sqrt{N_j}} \langle \alpha_h' | \vec{u}^{(j)} \cdot \vec{D} | \alpha_h \rangle, \tag{6}$$

where $N_j = \|\vec{u}^{(j)}\|$ is a normalization constant.

We consider infinite cylindrical core-shell nanowires with core radius a and shell radius b, so that the shell thickness is given by $b - a$. We choose the axis of the wire along the z direction of the cylindrical coordinates (r,θ,z). In the framework of the envelope function formalism for the 4×4 Luttinger Hamiltonian [30] in the axial approximation, and taking into account stress effects due to lattice mismatch [21,31,32], the fourfold wave function of the Γ_8 valence band

states can be expressed as

$$\langle \vec{r}|\alpha_h\rangle = \begin{pmatrix} F^{(1)}_{\nu_h}(r)|\upsilon_{3/2}\rangle \\ F^{(2)}_{\nu_h+1}(r)e^{i\theta}|\upsilon_{1/2}\rangle \\ F^{(3)}_{\nu_h+2}(r)e^{2i\theta}|\upsilon_{-1/2}\rangle \\ F^{(4)}_{\nu_h+3}(r)e^{3i\theta}|\upsilon_{-3/2}\rangle \end{pmatrix} e^{i(k_h z+\nu_h\theta)}. \quad (7)$$

Here, each component of the spinor is characterized by the set of quantum numbers $\alpha_h = (\nu_h, l_h, k_h)$, where ν_h is the z component of the angular momentum, l_h is the radial quantum number, and k_h is the z component of the wave vector. Functions $F^{(i)}_{\nu_h}(r) = A^{(i)}_{\nu_h} J_{\nu_h}(r)$ $(i = 1,\ldots,4)$ for $r < a$ and $F^{(i)}_{\nu_h}(r) = B^{(i)}_{\nu_h} J_{\nu_h}(r) + C^{(i)}_{\nu_h} N_{\nu_h}(r)$ for $a < r < b$, where $J_{\nu_h}(r)$, $N_{\nu_h}(r)$ are the Bessel and Neumann functions [33]. The constants $A^{(i)}_{\nu_h}, B^{(i)}_{\nu_h}, C^{(i)}_{\nu_h}$ and energy $E_{\nu_h,l_h}(k_h)$ are determined by the matching boundary conditions at $r = a$ and $r = b$. In consequence, the scattering matrix elements (6) can be cast as

$$M^{(j)}_{\alpha'_h,\alpha_h} = \frac{1}{\sqrt{N_j}} \left\langle \begin{pmatrix} F^{(1)}_{\nu'_h}(r)|\upsilon_{3/2}\rangle \\ F^{(2)}_{\nu'_h+1}(r)e^{i\theta}|\upsilon_{1/2}\rangle \\ F^{(3)}_{\nu'_h+2}(r)e^{2i\theta}|\upsilon_{-1/2}\rangle \\ F^{(4)}_{\nu'_h+3}(r)e^{3i\theta}|\upsilon_{-3/2}\rangle \end{pmatrix} \right| \vec{u}^{(j)} \cdot \vec{D} e^{i(\nu_h-\nu'_h)\theta} \left| \begin{pmatrix} F^{(1)}_{\nu_h}(r)|\upsilon_{3/2}\rangle \\ F^{(2)}_{\nu_h+1}(r)e^{i\theta}|\upsilon_{1/2}\rangle \\ F^{(3)}_{\nu_h+2}(r)e^{2i\theta}|\upsilon_{-1/2}\rangle \\ F^{(4)}_{\nu_h+3}(r)e^{3i\theta}|\upsilon_{-3/2}\rangle \end{pmatrix} \right\rangle \delta_{k'_h,k_h\pm k_z}, \quad (8)$$

where the momentum conservation along the z direction is written explicitly. The influence of the geometric factors, as well as the strain and bulk parameters on the matrix elements (8), are embedded in the phonon dispersion relations and the corresponding displacement vectors.

III. PHENOMENOLOGICAL CONTINUUM APPROACH IN CYLINDRICAL GEOMETRY

In order to derive a comprehensive expression for the electron-phonon DP matrix elements (8), it is required to discuss the phonon dispersion relations as a function of radii a and b, wave vector k_z, and influence of the strain effects across the core-shell surface, as well as the spatial symmetry properties of the phonon displacement vector. In the following, we study the confined phonon frequencies, the mixing of phonon modes as a consequence of the cylindrical spatial geometry, and their corresponding displacement vector, based on a unified macroscopic continuum theory where the medium properties are considered to be piecewise [34,35].

A. Equations of motion and basis for the solutions

Although the continuum approach employed in this work has been reported elsewhere [25,27,36,37], for the sake of completeness and further applications focusing on the electron-phonon DP Hamiltonian, we briefly recall the main features of the model, in particular, for nonpolar media and cylindrical core-shell geometry. Considering a harmonic time dependence for the oscillations, the equations of motion for the optical modes in an isotropic nonpolar media are given by [38]

$$\left(\omega^2 - \omega_0^2\right)\vec{u} = \beta_L^2 \nabla(\nabla\cdot\vec{u}) - \beta_T^2 \nabla\times\nabla\times\vec{u}. \quad (9)$$

In these expressions, β_L and β_T describe the quadratic dispersions of the LO- and TO-bulk phonon branches of the optical modes in the long-wave limit, respectively. Applying the Helmholtz's method of potentials [27,36,39], one can find a general basis of solutions for the problem, namely,

$$\vec{u}_{T1} = \begin{pmatrix} \frac{ik_z}{q_T} f_n'(q_T r) \\ -\frac{nk_z}{q_T}\frac{1}{q_T r} f_n(q_T r) \\ f_n(q_T r) \end{pmatrix} e^{i(n\theta+k_z z)},$$

$$\vec{u}_{T2} = \begin{pmatrix} \frac{in}{q_T r} f_n(q_T r) \\ -f_n'(q_T r) \\ 0 \end{pmatrix} e^{i(n\theta+k_z z)}, \quad (10)$$

$$\vec{u}_L = \begin{pmatrix} f_n'(q_L r) \\ \frac{in}{q_L r} f_n(q_L r) \\ \frac{ik_z}{q_L} f_n(q_L r) \end{pmatrix} e^{i(n\theta+k_z z)},$$

where the vector components are in cylindrical coordinates, (u_r, u_θ, u_z); the prime denotes the derivative with respect to the argument; n is an integer label related to the angular dependence of the modes; k_z is the continuum wave vector along the cylinder axis; and the wave vectors $q_{L,T}$ are given by

$$q^2_{L,T} = \frac{\omega_0^2 - \omega^2}{\beta^2_{L,T}} - k_z^2. \quad (11)$$

If $q^2_{L,T} > 0$ $(q^2_{L,T} < 0)$ and $r < a$, the function $f_n = J_n$ (I_n) order-n Bessel (infield) function. For $a < r < b$, f_n is a linear combination of J_n or Neumann N_n functions (I_n or MacDonald K_n). It is straightforward to check that the longitudinal solution verifies $\nabla\times\vec{u}_L = \vec{0}$, whereas the transverse solutions satisfy $\nabla\cdot\vec{u}_{T1} = \nabla\cdot\vec{u}_{T2} = 0$, as they should be. Particular cases of this basis have been used to study phonon modes in nonpolar nanotubes [36,40] and in solid nanowires with only one material at $k_z = 0$ [34,35].

In cylindrical geometry, neither the amplitudes $\vec{u}_{T1}$, $\vec{u}_{T2}$, nor $\vec{u}_L$ represent independent solutions for the phonon modes of the core-shell nanostructures. Nevertheless, the explicit form of the basis (10) allows us to elucidate the uncoupled modes and their polarization for special symmetries, such as $n = 0$ or $k_z = 0$.

A direct evaluation of Eq. (8) requires one to obtain the general solution of the problem. This solution can be written as a linear combination of the basis vectors (10), whose coefficients are determined by imposing the appropriate boundary conditions. If the bulk optical frequencies of core and shell materials are very different, it is a valid assumption that states are completely confined in the core or in the shell regions. This approach is fulfilled for Si and Ge, whose characteristic optical phonon frequencies are 521 and 301 cm^{-1}, respectively [41]. In addition, we will assume a large separation between the optical branches of shell and the

host material. Thus, the amplitude of the oscillations should be zero at the surfaces S ($r = a$ and $r = b$), i.e., $\vec{u}|_S = 0$.

B. Strain-induced shift of bulk modes

Core-shell silicon and germanium NWs should present large strain fields due to the lattice mismatch at the interface. This effect has been measured by Raman spectroscopy [5,8,22], as well as the strain-induced frequency shift as a function of core radius and shell thickness [6]. The frequency shift can be estimated by solving the secular equation [42]

$$\begin{vmatrix} p\varepsilon_{11} + q\widetilde{\varepsilon}_{11} - \lambda & 2t\varepsilon_{12} & 2t\varepsilon_{13} \\ 2t\varepsilon_{21} & p\varepsilon_{22} + q\widetilde{\varepsilon}_{22} - \lambda & 2t\varepsilon_{23} \\ 2t\varepsilon_{31} & 2t\varepsilon_{32} & p\varepsilon_{33} + q\widetilde{\varepsilon}_{33} - \lambda \end{vmatrix} = 0, \tag{12}$$

where p, q, and t are the phonon deformation potential values, ε_{ij} $(i,j = 1,2,3)$ the strain components in Cartesian coordinates, $\widetilde{\varepsilon}_{ii} = \mathrm{tr}\{\varepsilon\} - \varepsilon_{ii}$, $\mathrm{tr}\{\varepsilon\}$ is the trace of the strain tensor, and $\lambda = \omega^2 - \omega_0^2$ is the strain-induced frequency shift. In the present work we will deal with nanowires grown along the [011] direction. A detailed procedure for the evaluation of the shift λ in the above-mentioned crystallographic direction and analytical expressions for $\varepsilon_{ij}^{\mathrm{core}}$ and $\varepsilon_{ij}^{\mathrm{shell}}$ are given in Refs. [22,43]. Here we present the corresponding solutions,

$$\begin{aligned} \lambda_L &= \left(\tfrac{3}{4}p + \tfrac{5}{4}q + \tfrac{1}{2}t\right)\varepsilon_{rr}^{\mathrm{core}} + \left(\tfrac{1}{4}p + \tfrac{3}{4}q - \tfrac{1}{2}t\right)\varepsilon_{zz}^{\mathrm{core}}, \\ \lambda_{T1} &= \left(\tfrac{1}{2}p + \tfrac{3}{2}q - t\right)\varepsilon_{rr}^{\mathrm{core}} + \left(\tfrac{1}{2}p + \tfrac{1}{2}q + t\right)\varepsilon_{zz}^{\mathrm{core}}, \\ \lambda_{T2} &= \left(\tfrac{3}{4}p + \tfrac{5}{4}q + \tfrac{1}{2}t\right)\varepsilon_{rr}^{\mathrm{core}} + \left(\tfrac{1}{4}p + \tfrac{3}{4}q - \tfrac{1}{2}t\right)\varepsilon_{zz}^{\mathrm{core}}. \end{aligned} \tag{13}$$

Notice that the frequency shift in the core only depends on the ratio $\gamma = b/a$, and not on the particular values of the core and shell radii. However, for the shell, $\varepsilon_{rr}^{\mathrm{shell}}$ and $\varepsilon_{\theta\theta}^{\mathrm{shell}}$ depend on the coordinate r. For this reason, $\lambda_1^{\mathrm{shell}}$ and $\lambda_2^{\mathrm{shell}}$ are nontrivial functions of r and θ. As in this work we focus on core modes, it is sufficient with the expressions (13) shown above.

Studies by Raman spectroscopy prove that strain is partially relaxed, at least for the core diameters experimentally obtained to this date. In order to model this effect, Singh *et al.* [5] introduced an axial relaxation parameter ρ in the misfit factor, $\varepsilon_m = \varepsilon_{zz}^{\mathrm{core}} - \varepsilon_{zz}^{\mathrm{shell}}$. In the framework of this heuristic approach, the misfit strain is rewritten as $\varepsilon_m \to \varepsilon_m(1-\rho)$. This parameter varies between 0 and 1, so that when $\rho = 0$, the system is fully strained. Since all the experimental information available up to now deals with nanowires with partially relaxed strain, we take for our numerical evaluations a relaxation parameter $\rho = 0.5$, avoiding the unrealistic overestimation of the strain. The results for fully strained NWs are very similar, save for the larger shift due to strain effects.

Once the phonon bulk frequencies are corrected including strain through the replacement $\omega_0^2 \to \omega_0^2 + \lambda_i$ $(i = L,T1,T2)$ in the corresponding expressions (11), we calculate the phonon dispersion relations using Eq. (14). In the following, we address some numerical results focusing on the higher symmetry modes.

IV. DISPERSION RELATIONS FOR CORE-SHELL NANOWIRES

We study the core modes in Ge-Si and Si-Ge systems and, in particular, we analyze the coupling for different values of n and k_z, as well as the frequency shift due to confinement as a function of the core and shell radii a, b, and the wave vector k_z. Taking a linear combination of the basis functions (10) and applying the boundary condition $\vec{u}|_{r=a} = 0$, the general dispersion relations for core phonons are obtained by solving the transcendental equation

$$\begin{aligned} &J_n(\mu_{T1})\left[J_n'(\mu_L)J_n'(\mu_{T2}) - \frac{n^2}{\mu_L\mu_{T2}}J_n(\mu_L)J_n(\mu_{T2})\right] \\ &\quad = \frac{\widetilde{k}_z^2}{\mu_L\mu_{T1}}J_n(\mu_L)\left[J_n'(\mu_{T1})J_n'(\mu_{T2})\right. \\ &\qquad \left. - \frac{n^2}{\mu_{T1}\mu_{T2}}J_n(\mu_{T1})J_n(\mu_{T2})\right], \end{aligned} \tag{14}$$

where $\widetilde{k}_z = k_z a$ and $\mu_i^2 = q_i^2 a^2 + \lambda_i(\gamma)a^2/\beta_i^2$ $(i = L,T1,T2)$.

From the above equation, immediately we obtain the following symmetry properties: (i) for $n = 0$ and $k_z = 0$, the triple degeneracy of the optical modes is broken, and we have three independent subsets of confined modes for L, $T1$, and $T2$; (ii) for $n \neq 0$ and $k_z = 0$, the degeneracy is partially lifted: L and $T2$ modes are coupled, while $T1$ remains uncoupled;

(iii) for $n = 0$ with $k_z \neq 0$, the bulk degeneracy is also split into two subsets, one belonging to the independent transversal $T2$ phonon mode, and the other corresponding to the coupled longitudinal and transverse $L - T1$ modes; and finally, (iv) for $n \neq 0$ and $k_z \neq 0$ all the L, $T1$, and $T2$ phonon vector amplitudes are mixed.

These results, stemming from the peculiarities of the cylindrical geometry, have profound consequences on the EPH. According to these symmetries, which are characterized by the azimuthal label n and wave vector k_z, four different physical situations can be distinguished in relation to the EPH, which will be of use to analyze subsequent calculations of the dispersion relations for core-shell Ge-Si and Si-Ge NWs.

Table I shows the input parameters employed in the calculations. In the following the values given in Table I are assumed to be size independent, a hypothesis that should not be valid for very small radii. Dimensionless quadratic curvature parameters for the transversal (β_T^2) and longitudinal (β_L^2) bulk optical phonon bands, along the [011] crystallographic direction used here, are 6.33×10^{-12}, 11.53×10^{-12} and 17.59×10^{-12}, 31.95×10^{-12} for Ge and Si, respectively.

TABLE I. Bulk parameters for Ge and Si with diamond structure. ω_0 is given in cm^{-1}, the Young's modulus E in 10^{12} $\mathrm{dyn/cm}^2$, and the lattice constant a_0 in nanometers.

	ω_0	p/ω_0^2	q/ω_0^2	t/ω_0^2	E	ν	a_0
Ge	301[a]	−1.47[b]	−1.93[b]	−1.11[b]	1.28[c]	0.21[c]	0.566[c]
Si	521[a]	−1.83[b]	−2.33[b]	−0.71[b]	1.59[c]	0.23[c]	0.543[c]

[a]Reference [41].
[b]Reference [42].
[c]Reference [48].

These values have been fitted to the neutron dispersion data collected in Ref. [44], originally reported in Refs. [45,46] (Si) and [47] (Ge). As is well known, the transversal optical phonons are nondegenerate along the [011] crystallographic direction, showing different β_{T1} and β_{T2} curvatures. For Si and Ge bulk semiconductors $\beta_{T1} \approx \beta_{T2}$. Thus, in the framework of the isotropic approximation, we have chosen for β_T the average between β_{T1} and β_{T2} values.

A. Modes with $n = 0$ and $k_z = 0$

First, we focus on the uncoupled modes with $n = 0$ and $k_z = 0$. By inspection of the basis for the solutions, it is clear that for this case all modes L, $T1$, and $T2$ are completely decoupled. By imposing the boundary condition of complete confinement, the frequencies of core modes are found to be

$$\begin{aligned}
\omega_L^2 &= \omega_0^2 - \frac{\beta_L^2 \left(\mu_1^{(m)}\right)^2}{a^2} + \lambda_L(\gamma), \\
\omega_{T1}^2 &= \omega_0^2 - \frac{\beta_T^2 \left(\mu_0^{(m)}\right)^2}{a^2} + \lambda_{T1}(\gamma), \\
\omega_{T2}^2 &= \omega_0^2 - \frac{\beta_T^2 \left(\mu_1^{(m)}\right)^2}{a^2} + \lambda_{T2}(\gamma),
\end{aligned} \tag{15}$$

where $\mu_i^{(m)}$ $(i = 0,1)$ are the roots of $J_i(\mu_i^{(m)}) = 0$, with $m = 1,2,\ldots$.

The second term in the right-hand side of Eqs. (15) gives the effect of confinement. Obviously, it is always negative, producing a downshift of the modes. The confinement term for these uncoupled modes varies with $1/a^2$. The third term is the effect of strain, λ_i, which depends on the ratio γ and the crystallographic direction.

In the present case, $H_{\text{e-ph}}$ is decoupled into three independent Hamiltonians, $H_{\text{e-ph}}^{L}$, $H_{\text{e-ph}}^{T1}$, and $H_{\text{e-ph}}^{T2}$, which characterize the three orthogonal phonon displacements along the radial ($\hat{e}_r$), axial ($\hat{e}_z$), and azimuthal ($\hat{e}_\theta$) directions, respectively.

Figure 1 shows the core modes as a function of the core radius a in a core-shell system for fixed shell thickness. The left panel presents the Ge-Si case, and the right panel depicts results for the Si-Ge nanowire. Recall that the role of the shell is essential to obtain the shift of the core bulk frequency, as explained in Sec. III B but, besides that, it does not play any role for the core modes, due to the boundary condition of complete confinement. There is an overall increase of the core mode frequencies in the left panel of Fig. 1, in which Ge is the core material, while the modes are downshifted in the right panel of Fig. 1, where Si is the core medium. This is related to the difference of lattice constants: as can be seen in Table I, the lattice constant of Si is smaller than that of Ge, thus the strain always produces a redshift in the Si region of the wire, and a blueshift in the Ge part, no matter whether they constitute the core or the shell. The highest frequency mode of the Ge-core case (left panel) shows an increase of frequency for diminishing a in a substantial radius range, which indicates the importance of strain for this mode. Comparison of the results of Fig. 1 to the frequencies obtained for fixed shell/core ratio γ (not shown) allows us to conclude that for increasing values of a and fixed shell thickness, the frequencies tend to the bulk core value, whereas for γ fixed confinement effects disappear,

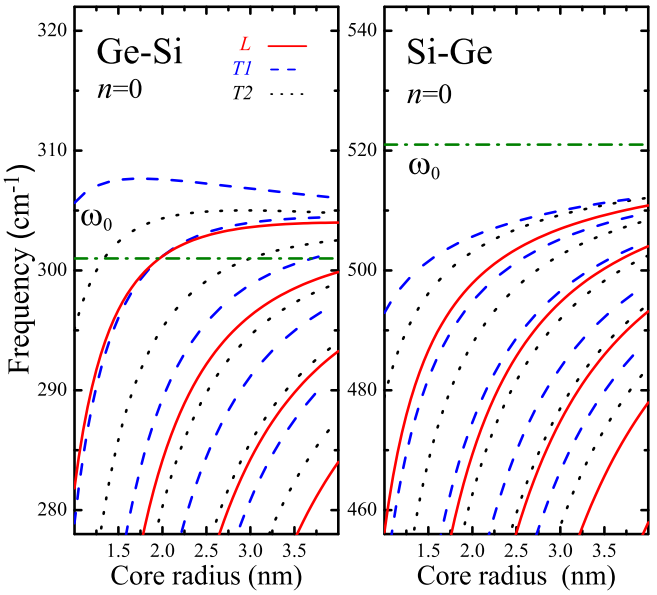

FIG. 1. (Color online) Frequencies of the core modes with $n = 0$ and $k_z = 0$ as a function of the core radius a in a core-shell system grown in the [011] direction. Left panel: Ge-Si. Right panel: Si-Ge, for fixed shell thickness $b - a = 1$ nm.

leaving the strain as the main contribution. As in Fig. 1, Ge core modes are blueshifted due to strain, whereas the Si modes are redshifted. The higher frequency mode of this latter panel also shows a blueshift for diminishing radius, which signals the prevalence of strain effects for this mode.

In a nanowire with fixed core radius, the frequency dependence is due to the strain, which varies with the shell radius via the ratio γ. As discussed above, the NW with Ge core always shows an increasing blueshift of all modes with increasing strain, due to the smaller Si lattice constant. For the same reason, all modes of strained Si-core NWs are redshifted.

B. Modes with $n \neq 0$ and $k_z = 0$

In the case of modes without axial symmetry, i.e., $n \neq 0$, we find for $k_z = 0$ that L and $T2$ modes are coupled, while the $T1$ mode remains uncoupled. The dispersion relation for the latter is given by

$$\omega_{T1}^2 = \omega_0^2 - \frac{\beta_T^2 \left(\mu_n^{(m)}\right)^2}{a^2} + \lambda_{T1}(\gamma), \tag{16}$$

where $J_n(\mu_n^{(m)}) = 0$ with $m = 1,2,\ldots$. The coupled $L - T2$ modes fulfill the equation

$$J_n'(\mu_L) J_n'(\mu_{T2}) - \frac{n^2}{\mu_L \mu_{T2}} J_n(\mu_L) J_n(\mu_{T2}) = 0, \tag{17}$$

with

$$\mu_L^2 = \left[\omega_0^2 + \lambda_L(\gamma) - \omega^2\right] \left(\frac{a}{\beta_L}\right)^2, \tag{18}$$

$$\mu_{T2}^2 = \left[\omega_0^2 + \lambda_{T2}(\gamma) - \omega^2\right] \left(\frac{a}{\beta_T}\right)^2. \tag{19}$$

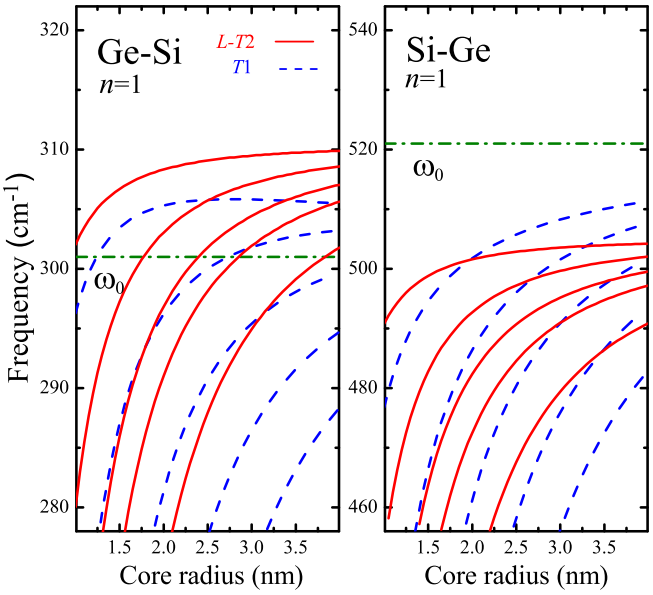

FIG. 2. (Color online) The same as Fig. 1 for $n = 1$.

Here we have only two independent blocks in the EPH. One corresponds to $H_{\text{e-ph}}^{T1}$ and the other to a mixture of u_L and u_{T2} amplitudes, with phonon polarization vector on the $(\hat{e}_r, \hat{e}_\theta)$ plane, which leads to $H_{\text{e-ph}}^{L-T2}$. Figure 2 shows the core modes with $n = 1$ and $k_z = 0$ as a function of the core radius for fixed shell thickness. Notice that the uncoupled $T1$ modes behave as for the $n = 0$ case. The coupled $L - T2$ modes are closer in frequencies compared to the $n = 0$ case. This behavior holds for varying core radius if the same shell/core ratio is maintained.

C. Modes with $n = 0$ and $k_z \neq 0$

Now we consider the dependence of the mode frequencies with the wave vector, $k_z \neq 0$. We focus on the $n = 0$ modes that results in an uncoupled $T2$ mode and coupled $L - T1$ mode. The uncoupled transverse mode is given by $J_1(\mu_1^{(m)}) = 0$, which leads to the dispersion relation

$$\omega_{T2}^2 = \omega_0^2 - \frac{\beta_T^2 \left(\mu_1^{(m)}\right)^2}{a^2} + \lambda_{T2}(\gamma) - \beta_T^2 k_z^2. \tag{20}$$

Equation (20) is just like the bulk dispersion relation, except for the shifts due to the spatial confinement $(\beta_T \mu_1^{(m)})^2/a^2$ and the strain, $\lambda_{T2}(\gamma)$. The coupled $L - T1$ modes are obtained from Eq. (21):

$$J_0'(\mu_L) J_0(\mu_{T1}) - \frac{\widetilde{k}_z^2}{\mu_L \mu_{T1}} J_0(\mu_L) J_0'(\mu_{T1}) = 0, \tag{21}$$

with

$$\mu_L^2 = \left[\omega_0^2 + \lambda_L(\gamma) - \omega^2\right] \left(\frac{a}{\beta_L}\right)^2 - \widetilde{k}_z^2, \tag{22}$$

$$\mu_{T1}^2 = \left[\omega_0^2 + \lambda_{T1}(\gamma) - \omega^2\right] \left(\frac{a}{\beta_T}\right)^2 - \widetilde{k}_z^2. \tag{23}$$

If $k_z \neq 0$, the axial symmetry is broken and for $n = 0$, the amplitudes u_L and u_{T1} are coupled, so we obtain the $H_{\text{e-ph}}^{L-T1}$ which describes the electronic interaction with phonons polarized on the $(\hat{e}_r, \hat{e}_z)$ plane. In addition, we have a $H_{\text{e-ph}}^{T2}$ term for the uncoupled $T2$ optical modes.

V. ELECTRON-OPTICAL PHONON SCATTERING RATE

As stated above, near the Γ point of the Brillouin zone the conduction band does not play a role in the electron-optical phonon deformation potential Hamiltonian, and the hole states are the only contribution to $H_{\text{e-ph}}$. Hence, it becomes important to understand how the structure of the $H_{\text{e-ph}}$ is unfolded by the symmetry properties of the degenerate valence bands in NWs with cylindrical geometry. Notice that the influence of the geometric factors, as well as the strain and bulk parameters on the hole-phonon matrix elements (8) are embedded in the phonon dispersion relations and the corresponding phonon displacement vector. Hence, on the basis of the calculated frequencies and phonon amplitudes, explicit expressions for the DP matrix elements (6) can be carried forward. From Eq. (8) and the previous discussions, it becomes clear that the hole-phonon scattering rate depends on the phonon polarization. Since we are in a cylindrical geometry, it is not possible to decouple the phonon modes in a set of three independent polarizations. In the following sections we illustrate some cases of interest for the hole scattering caused by the phonon polarization along the axial, radial, and azimuthal directions.

A. Phonon modes polarized along the growth direction

For phonon modes polarized along the cylinder axis, we have to consider the z component of the vector amplitude $\vec{u}^{(j)}$. Thus, from the basis vectors shown in Eq. (10) we have

$$u_z^{(\hat{e}_z)} = U_z e^{in\theta} = [J_n(\mu_{T1} r/a) J_n(\mu_L) - J_n(\mu_L r/a) J_n(\mu_{T1})] \times e^{in\theta}/\sqrt{N_z}\,. \tag{24}$$

Consequently, combining Eqs. (4) and (7), the amplitude (8) can be cast as

$$M_{\alpha_h', \alpha_h}^{(\hat{e}_z)} = \frac{i d u_0}{a_0} \left(\delta_{\nu_h', \nu_h + n + 2} \left[-\left\langle F_{\nu_h'}^{(1)} \middle| U_z \middle| F_{\nu_h + 2}^{(3)} \right\rangle - \left\langle F_{\nu_h' + 1}^{(2)} \middle| U_z \middle| F_{\nu_h + 3}^{(4)} \right\rangle\right] + \delta_{\nu_h', \nu_h + n - 2} \left[\left\langle F_{\nu_h' + 2}^{(3)} \middle| U_z \middle| F_{\nu_h}^{(1)} \right\rangle + \left\langle F_{\nu_h' + 3}^{(4)} \middle| U_z \middle| F_{\nu_h + 1}^{(2)} \right\rangle\right]\right) \delta_{k_h', k_h \pm k_z}. \tag{25}$$

This scattering rate is ruled by the combination of longitudinal L and transverse $T1$ amplitudes. In the particular case of $k_z = 0$, as is required, for example, in infrared spectroscopy measurements, the hole transition is assisted by a pure transversal $T1$ optical phonon. Figure 3 shows the contribution of the amplitude u_z to the $H_{\text{e-ph}}^{(\hat{e}_z)}$. The left panel is devoted to the three first modes $(m = 1, 2, 3)$ with $n = 0, 1$ and $k_z = 0$. Notice that the u_z is independent of the core-shell materials involved. The right panel presents the elongation for $n = 0$ and $k_z \neq 0$ for Ge-Si and Si-Ge NWs.

B. Polarization along the radial direction

The vector component $u_r^{(\hat{e}_r)}$ is a mixture of the three amplitudes u_L, u_{T1}, and u_{T2}; thus, employing Eq. (10) we

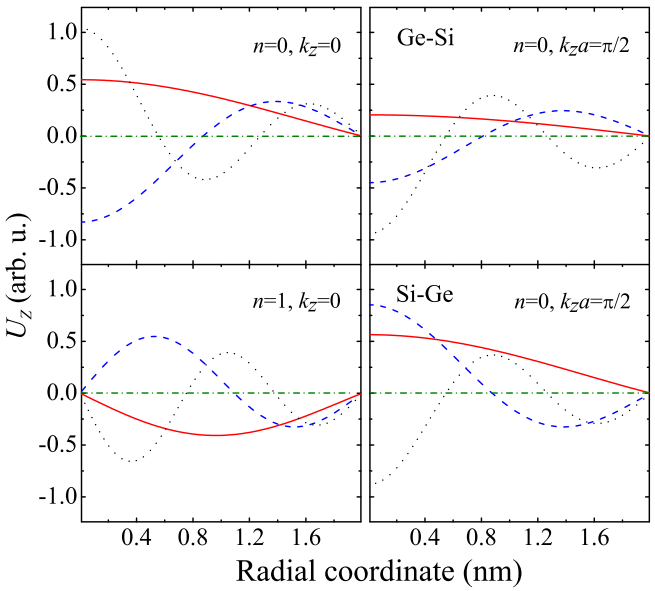

FIG. 3. (Color online) Core phonon amplitude U_z for Ge-Si and Si-Ge core-shell NWs. Left panel: $n = 0$, 1, and $k_z = 0$. Right panel: $n = 0$ and $k_z a = \pi/2$. In the calculation $a = 2$ nm and $b = 4$ nm.

have

$$u_r^{(\hat{e}_r)} = U_r e^{in\theta} = [A_{T2} J_n'(\mu_{T2} r/a) + A_{T1} J_n(\mu_{T1} r/a) + J_n'(\mu_L r/a)] e^{in\theta}/\sqrt{N_r}, \quad (26)$$

where the constants A_{T1} and A_{T2} are given in Appendix B. This allows us to reduce the matrix elements (8) to

$$M^{(\hat{e}_r)}_{\alpha_h',\alpha_h} = \frac{du_0}{a_0}\big(\delta_{\nu_h',\nu_h+n+2}\big[-\langle F^{(1)}_{\nu_h'}|U_r|F^{(2)}_{\nu_h+1}\rangle + \langle F^{(3)}_{\nu_h'+2}|U_r|F^{(4)}_{\nu_h+3}\rangle\big] + \delta_{\nu_h',\nu_h+n-2}\big[-\langle F^{(2)}_{\nu_h'+1}|U_r|F^{(1)}_{\nu_h}\rangle + \langle F^{(4)}_{\nu_h'+3}|U_r|F^{(3)}_{\nu_h+2}\rangle\big]\big)\delta_{k_h',k_h\pm k_z}. \quad (27)$$

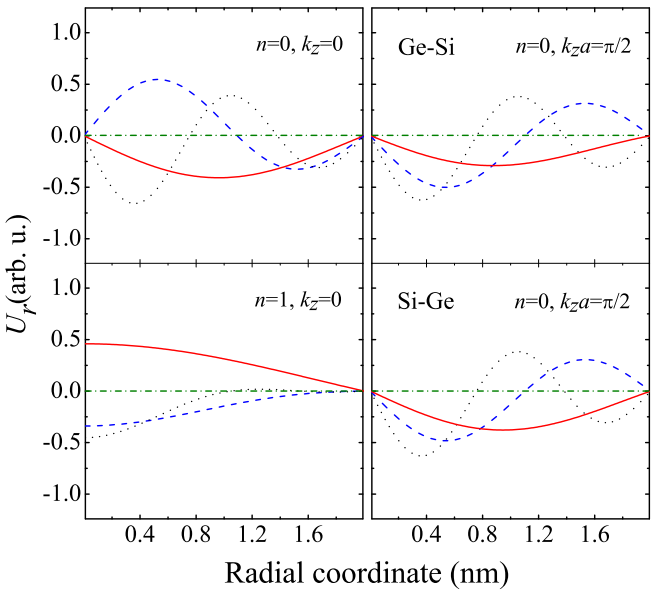

FIG. 4. (Color online) Same as in Fig. 3 for core phonon amplitude U_r.

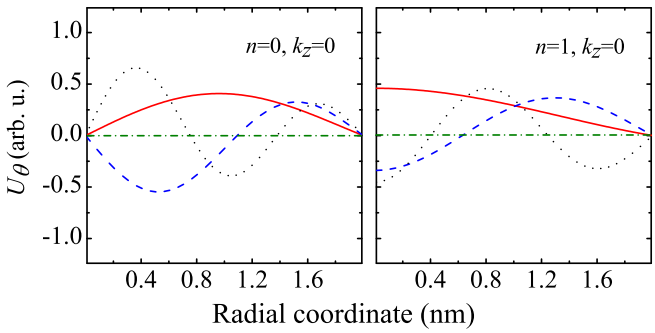

FIG. 5. (Color online) Core phonon amplitude U_θ for Ge-Si and Si-Ge core-shell NW and $k_z = 0$. Left panel: $n = 0$. Right panel: $n = 1$. In the calculation $a = 2$ nm and $b = 4$ nm.

Notice that even for $k_z = 0$ the $H^{(\hat{e}_r)}_{\text{e-ph}}$ presents a mixture of the $L - T2$ modes. Only for $n = 0$ is there a pure longitudinal oscillation along the radial direction.

C. Polarization along the azimuthal direction

From the basis given in Eq. (10) we have

$$u_\theta^{(\hat{e}_\theta)} = U_\theta e^{in\theta} = [B_{T1} J_n(\mu_{T1} r/a) - J_n'(\mu_{T2} r/a) + B_L J_n(\mu_L r/a)] e^{in\theta}/\sqrt{N_\theta}, \quad (28)$$

where the coefficients B_{T1} and B_L are reported in Appendix B. With this latter expression, the scattering matrix element with a deformation potential $D_{(\hat{e}_\theta)}$ becomes

$$M^{(\hat{e}_\theta)}_{\alpha_h',\alpha_h} = \frac{idu_0}{a_0}\big(\delta_{\nu_h',\nu_h+n+2}\big[-\langle F^{(1)}_{\nu_h'}|U_\theta|F^{(2)}_{\nu_h+1}\rangle + \langle F^{(3)}_{\nu_h'+2}|U_\theta|F^{(4)}_{\nu_h+3}\rangle\big] + \delta_{\nu_h',\nu_h+n-2}\big[\langle F^{(2)}_{\nu_h'+1}|U_\theta|F^{(1)}_{\nu_h}\rangle - \langle F^{(4)}_{\nu_h'+3}|U_\theta|F^{(3)}_{\nu_h'+2}\rangle\big]\big)\delta_{k_h',k_h\pm k_z}. \quad (29)$$

The dependence on r of the phonon elongations U_r and U_θ which appear in $H^{(\hat{e}_r)}_{\text{e-ph}}$ and $H^{(\hat{e}_\theta)}_{\text{e-ph}}$ are shown in Figs. 4 and 5, respectively. For both Si-Ge and Ge-Si NWs we take $n = 0,1$, $k_z a = 0, \pi/2$ and $m = 1,2,3$.

Notice that the deformation potential scattering amplitudes (8) of the special reported cases given by Eqs. (25), (27), and (29) take into account the phonon symmetries of Ge-Si and Si-Ge NWs and the corresponding strain effects. All information about the shell structure is carried out in the calculated phonon frequency $\omega_{m,n} = \omega_{m,n}[a, \lambda_i(\gamma)]$.

VI. CONCLUSIONS

In this work we present a study of the nonpolar zone-center optical phonons and the electron-phonon deformation potential interaction in core-shell cylindrical nanowires. The vector phonon displacement field $\vec{U}$ is derived by solving a system of coupled differential equations providing a general basis for the solutions of the problem. It is found that the modes show mixed torsional, axial, and radial characters, depending on the physical conditions involved. Thus, in general, the $H_{\text{e-ph}}$ cannot be decoupled into pure transversal or longitudinal motions depending on the phonon propagation direction with respect to the nanowire axis.

An important application of the above developed theory is the Raman selection rules. The first-order phonon resonant Raman tensor of a core/shell NW is proportional to the scattering amplitude [49], $\mathcal{M}_{FI}$, between the initial ($|I\rangle$) and final ($|F\rangle$) states as given by

$$\mathcal{M}_{FI} \sim \sum_{\mu_1\mu_2} \frac{\langle F|\,\hat{e}_F\cdot\vec{p}\,|\mu_2\rangle\,\langle\mu_2|\,H_{\text{e-ph}}\,|\mu_1\rangle\,\langle\mu_1|\,\hat{e}_I\cdot\vec{p}\,|I\rangle}{(\hbar\omega_s - E_{\mu_2})(\hbar\omega_l - E_{\mu_1})}, \tag{30}$$

where ω_l ($\omega_s = \omega_l - \omega_{m,n}$) is the incident frequency light (Stokes Raman shift with a phonon of frequency $\omega_l - \omega_{m,n}$) and polarization $\hat{e}_I$ ($\hat{e}_S$), $\vec{p}$ is the single-particle momentum, and $|\mu_i\rangle = |\alpha_{ei}\rangle|\alpha_{hi}\rangle$ ($i = 1,2$) are the intermediate free-electron hole pair states with energy E_{μ_i}. Here, $|\alpha_e\rangle = |k_e,\nu_e\rangle|F_{\nu_e}\rangle|S\uparrow(\downarrow)\rangle$, with $|F_{\nu_e}\rangle$ being a proper combination of the cylindrical real Bessel functions as $r < a$ or $a < r < b$, and $|S\uparrow(\downarrow)\rangle$ is the Bloch function in the conduction band with spin parallel (antiparallel) to the NW axis along the z axis. By introducing the electron-hole wave functions and electron-phonon interaction given by Eqs. (2)–(4) [50], we are able to obtain the Raman selection rules. In the dipole approximation, where the phonon wave vector $k_z \approx 0$, and considering backscattering configuration from the quantum wire along the z-growth direction $\overline{Z}(\hat{e}_F,\hat{e}_I)Z$ [51], we choose the phonon propagating direction to be z with amplitude $u_z^{(\hat{e}_z)}$ and $H_{\text{e-ph}}^{T1}$ for the pure $T1$ transversal phonons. In this case, from Eq. (30) and taking into account the cylindrical symmetry of the electron-hole wave functions $|\mu_i\rangle$, it is possible to show that the DP interaction for the $T1$ confined phonon is Raman forbidden in any parallel $\hat{e}_F \| \hat{e}_I$ or perpendicular $\hat{e}_F \perp \hat{e}_I$ configurations. Notice that the $\omega_{n,m}^{T1}$ mode is IFP active with quantum number $n = 1$. Now, if we consider the scattering configuration $\overline{X}'(Y',Z)X'$, we are in the presence of a combination of L and $T2$ modes (see Sec. IV B) and EPH $H_{\text{e-ph}}^{L-T2}$ [52].

Regarding the Raman intensity, as long as the phonon amplitude U has typical dimensions scaling as the core size a, and the deformation coupling constant in Eqs. (2)–(4) is proportional to $a^{-3/2}$, the magnitude of deformation potential Hamiltonian will be proportional to $1/\sqrt{a}$. Hence, the Raman intensity increases as the core radius decreases, and in consequence the effects of the mechanical boundary conditions become important. Similar results have been reported and observed experimentally in spherical quantum dots [20].

For the case of dressed nonpolar Si-Ge based NWs with complete confinement, the shell has a role on the frequency shift of the core optical modes through the strain. The employed basis (10) for the solutions of the problem allows one to study the influence of the longitudinal and transversal mixture on $H_{\text{e-ph}}$ as a function of the confinement and wave vector k_z. We also give explicit analytical expressions of the $H_{\text{e-ph}}$ for the cases of torsional, axial, and radial phonon propagations. Moreover, electronic transitions in the valence are assisted by phonons if the angular momentum quantum numbers for the involved hole states fulfill the selection rule $\Delta\nu = n + 2$ related to the emission or absorption of one confined phonon.

Finally, for a complete treatment of the electron-phonon Hamiltonian, the evaluation of the overlapping integrals between the phonon vector displacement and electronic states become necessary. Nevertheless, the general structure of the fourfold wave function given by Eq. (8) and the symmetry properties discussed in Sec. V remain valid. This settles the basis for considering different effects on the electronic states as, for example, the influence of external fields and the electron-hole Coulomb interaction, among others. The present model allows for the study of optical phonon deformation potential as a function of the structural parameters, which contains crucial information for the characterization of core-shell nanowires.

ACKNOWLEDGMENTS

This work was partially supported by Spanish MINECO through Grant No. FIS2012-33521. D.G.S.-P., C.T.-G., and G.E.M. acknowledge support from the Brazilian Agencies FAPESP and CNPq. R.P.-A. acknowledges CONACyT (México) support through Grant No. 208108 and hospitality at ICMM-CSIC, Madrid, Spain.

APPENDIX A: DEFORMATION POTENTIAL

The electron-deformation potential Hamiltonian (5) is written as

$$u_{\hat{e}_x}(\mathbf{r})D_{\hat{e}_x}(\mathbf{r}) + u_{\hat{e}_y}(\mathbf{r})D_{\hat{e}_y}(\mathbf{r}) + u_{\hat{e}_z}(\mathbf{r})D_{\hat{e}_z}(\mathbf{r}). \tag{A1}$$

The matrix elements of Eq. (6), in terms of the envelope functions (7) and the valence band Bloch functions $v_j(\mathbf{r})$, are proportional to $\langle v_j(\mathbf{r})|\,\vec{D}(\mathbf{r})|v_i(\mathbf{r})\rangle$, where it is assumed a rapid spatial variation of the Bloch functions in the unit cell in comparison with the envelope functions $F_\nu^{(j)}(\mathbf{r})$. Hence, the deformation potential $\vec{D}(\mathbf{r})$ can be characterized by the matrix elements between valence-band-edge wave functions $|v_j\rangle$. For the diamond structure, the degenerate valence bands present Γ_8 symmetry at the Γ point of the Brillouin zone. The inclusion of the spin-orbit interaction splits the valence band degeneracy into fourfold $j = 3/2$, $m_Z = \pm 3/2, \pm 1/2$, and twofold $j = 1/2$, $m_Z = \pm 1/2$ degenerate states, with j the total angular momentum and m_Z the z component [53]. The fourfold multiplet $j = 3/2$ valence-band-edge wave functions are given by [54]

$$\begin{aligned}
|v_{-3/2}\rangle &= \frac{i}{\sqrt{2}}|(X - iY)\rangle|\downarrow\rangle,\\
|v_{-1/2}\rangle &= \frac{1}{\sqrt{6}}|(X - iY)\rangle|\uparrow\rangle + \sqrt{\frac{2}{3}}|Z\rangle|\downarrow\rangle,\\
|v_{1/2}\rangle &= \frac{i}{\sqrt{6}}|(X + iY)\rangle|\downarrow\rangle - i\sqrt{\frac{2}{3}}|Z\rangle|\uparrow\rangle,\\
|v_{3/2}\rangle &= \frac{1}{\sqrt{2}}|(X + iY)\rangle|\uparrow\rangle,
\end{aligned} \tag{A2}$$

where $|\uparrow\rangle$ ($|\downarrow\rangle$) denotes the spin parallel (antiparallel) to the growth direction z and the functions $|X\rangle$, $|Y\rangle$, and $|Z\rangle$ transform as atomic p-like functions. Under the symmetry operations of the representation Γ_8, the only nonzero elements of the deformation potential $\vec{D}$ are $\langle Y|D_x|Z\rangle$, $\langle Z|D_y|X\rangle$, $\langle Y|D_z|X\rangle$, and equivalents [49]. Thus, we have for each

component of $\vec{D}$ in matrix representation

$$D_{\hat{e}_x} = \frac{du_0}{a_0}\begin{pmatrix} 0 & -1 & 0 & 0 \\ -1 & 0 & 0 & 0 \\ 0 & 0 & 0 & 1 \\ 0 & 0 & 1 & 0 \end{pmatrix}, \tag{A3}$$

$$D_{\hat{e}_y} = \frac{idu_0}{a_0}\begin{pmatrix} 0 & -1 & 0 & 0 \\ 1 & 0 & 0 & 0 \\ 0 & 0 & 0 & 1 \\ 0 & 0 & -1 & 0 \end{pmatrix}, \tag{A4}$$

$$D_{\hat{e}_z} = \frac{idu_0}{a_0}\begin{pmatrix} 0 & 0 & -1 & 0 \\ 0 & 0 & 0 & -1 \\ 1 & 0 & 0 & 0 \\ 0 & 1 & 0 & 0 \end{pmatrix}. \tag{A5}$$

Now, under the unitary transformation

$$T = \begin{pmatrix} \cos\theta & \sin\theta & 0 \\ -\sin\theta & \cos\theta & 0 \\ 0 & 0 & 1 \end{pmatrix}, \tag{A6}$$

we transform Eq. (A1), and the tensor components $\vec{D}$ in cylindrical coordinates can be expressed in terms of the components D_i $(i = \hat{e}_r, \hat{e}_\theta, \hat{e}_z)$ as

$$\begin{aligned} D_{\hat{e}_r} &= \cos\theta D_{\hat{e}_x} + \sin\theta D_{\hat{e}_y}, \\ D_{\hat{e}_\theta} &= -\sin\theta D_{\hat{e}_x} + \cos\theta D_{\hat{e}_y}, \\ D_{\hat{e}_z} &= D_{\hat{e}_z}. \end{aligned} \tag{A7}$$

Equations (2)–(4) are derived from Eqs. (A7).

APPENDIX B: PHONON AMPLITUDES

The coefficients for the phonon elongation U_r in Eq. (26) are given by

$$A_{T1} = -\left(\frac{\widetilde{k}_z^2}{\mu_{T1}\mu_L}\frac{J_n(\mu_L)J_n'(\mu_{T2})}{J_n^2(\mu_{T1})} + \frac{J_n'(\mu_L)}{J_n(\mu_{T1})}\right) \tag{B1}$$

and

$$A_{T2} = \frac{\widetilde{k}_z^2}{\mu_{T1}\mu_L}\frac{J_n(\mu_L)}{J_n(\mu_{T1})}. \tag{B2}$$

For the amplitude U_θ in Eq. (28) we obtain

$$B_{T1} = \frac{\widetilde{k}_z^2}{\widetilde{k}_z^2 + \mu_{T1}^2}\frac{J_n'(\mu_{T2})}{J_n(\mu_{T1})}, \tag{B3}$$

$$B_L = \frac{\mu_{T1}^2}{\widetilde{k}_z^2 + \mu_{T1}^2}\frac{J_n'(\mu_{T2})}{J_n(\mu_L)}. \tag{B4}$$

[1] W. Lu and C. M. Lieber, J. Phys. D **39**, R387 (2006).
[2] O. Hayden, R. Agarwal, and W. Lu, Nano Today **3**, 12 (2008).
[3] N. P. Dasgupta, J. Sun, C. Liu, S. Brittman, S. C. Andrews, J. Lim, H. Gao, R. Yan, and P. Yang, Adv. Mater. **26**, 2137 (2014).
[4] L. J. Lauhon, M. S. Gudiksen, D. Wang, and C. M. Lieber, Nature (London) **420**, 57 (2002).
[5] R. Singh, C. D. Poweleit, E. Dailey, J. Drucker, and J. Menéndez, Semicond. Sci. Technol. **27**, 085008 (2012).
[6] D. C. Dillen, K. M. Varahramyan, C. M. Corbet, and E. Tutuc, Phys. Rev. B **86**, 045311 (2012).
[7] H. Kallel, A. Arbouet, G. BenAssayag, A. Chehaidar, A. Potié, B. Salem, T. Baron, and V. Paillard, Phys. Rev. B **86**, 085318 (2012).
[8] R. Singh, E. J. Dailey, J. Drucker, and J. Menéndez, J. Appl. Phys. **110**, 124305 (2011).
[9] D. Martínez-Gutiérrez and V. Velasco, Physica E **54**, 86 (2013).
[10] M. Hu, X. Zhang, K. P. Giapis, and D. Poulikakos, Phys. Rev. B **84**, 085442 (2011).
[11] X. Liu, J. Hu, and B. Pan, Physica E **40**, 3042 (2008).
[12] R. Peköz and J.-Y. Raty, Phys. Rev. B **80**, 155432 (2009).
[13] R. N. Musin and X.-Q. Wang, Phys. Rev. B **71**, 155318 (2005).
[14] M. K. Y. Chan, J. Reed, D. Donadio, T. Mueller, Y. S. Meng, G. Galli, and G. Ceder, Phys. Rev. B **81**, 174303 (2010).
[15] T. E. Trammell, X. Zhang, Y. Li, L.-Q. Chen, and E. C. Dickey, J. Cryst. Growth **310**, 3084 (2008).
[16] I. A. Goldthorpe, A. F. Marshall, and P. C. McIntyre, Nano Lett. **8**, 4081 (2008).
[17] C. Kloeffel, M. Trif, and D. Loss, Phys. Rev. B **90**, 115419 (2014).
[18] F. Maier and D. Loss, Phys. Rev. B **85**, 195323 (2012).
[19] Y. Hu, F. Kuemmeth, C. M. Lieber, and C. M. Marcus, Nat. Nanotechnol. **7**, 47 (2012).
[20] A. G. Rolo, M. I. Vasilevskiy, M. Hamma, and C. Trallero-Giner, Phys. Rev. B **78**, 081304 (2008).
[21] G. Bir and G. Pikus, *Symmetry and Strain-Induced Effects in Semiconductors*, A Halsted Press book (Wiley, New York, 1974).
[22] J. Menéndez, R. Singh, and J. Drucker, Ann. Phys. (Berlin) **523**, 145 (2011).
[23] M. C. Klein, F. Hache, D. Ricard, and C. Flytzanis, Phys. Rev. B **42**, 11123 (1990).
[24] S. Nomura and T. Kobayashi, Phys. Rev. B **45**, 1305 (1992).
[25] C. Trallero-Giner, R. Pérez-Álvarez, and F. García-Moliner, *Long Wave Polar Modes in Semiconductor Heterostructures*, 1st ed. (Pergamon Elsevier Science, London, 1998).
[26] D. G. Santiago-Pérez, C. Trallero-Giner, R. Pérez-Álvarez, L. Chico, R. Baquero, and G. E. Marques, J. Appl. Phys. **112**, 084322 (2012).
[27] D. G. Santiago-Pérez, C. Trallero-Giner, R. Pérez-Álvarez, and L. Chico, Physica E **56**, 151 (2014).
[28] O. Madelung, *Introduction to Solid State Theory* (Springer, Berlin, 1996).
[29] R. Martin, Phys. Rev. B **4**, 3676 (1971).
[30] J. M. Luttinger and W. Kohn, Phys. Rev. **97**, 869 (1955).

[31] S.-S. Li, J.-B. Xia, Z. L. Yuan, Z. Y. Xu, W. Ge, X. R. Wang, Y. Wang, J. Wang, and L. L. Chang, Phys. Rev. B **54**, 11575 (1996).
[32] C. Kloeffel, M. Trif, and D. Loss, Phys. Rev. B **84**, 195314 (2011).
[33] M. Abramowitz and I. Stegun, *Handbook of Mathematical Functions* (U.S. Goverment Printing Office, Washinton, DC, 1964).
[34] F. Comas, C. Trallero-Giner, and A. Cantarero, Phys. Rev. B **47**, 7602 (1993).
[35] F. Comas, A. Cantarero, C. Trallero-Giner, and M. Moshinsky, J. Phys.: Condens. Matter **7**, 1789 (1995).
[36] L. Chico and R. Pérez-Álvarez, Phys. Rev. B **69**, 035419 (2004).
[37] T. Thonhauser and G. D. Mahan, Phys. Rev. B **69**, 075213 (2004).
[38] This equation is straightforwardly derived from the hydrodynamic phenomenological model for cubic polar semiconductors described in Refs. [25,55] considering that the polarization and electric field associated with vibrations are zero. Note that since the core and shell bulk materials are nonpolar, $\omega_{\mathrm{TO}} = \omega_{\mathrm{LO}} = \omega_0$.
[39] P. M. Morse and H. Feshbach, *Methods of Theoretical Physics* (McGraw-Hill, New York, 1953).
[40] L. Chico, R. Pérez-Álvarez, and C. Cabrillo, Phys. Rev. B **73**, 075425 (2006).
[41] O. Madelung, *Physics of Group IV Elements and III-V Compounds* (Springer-Verlag, Berlin, 1982), Vol. 17a.
[42] E. Anastassakis and M. Cardona, in *High Pressure in Semiconductor Physics II*, edited by T. Suski and W. Paul (Academic, New York, 1998).
[43] D. G. Santiago Pérez, C. Trallero-Giner, R. Pérez-Álvarez, and L. Chico (unpublished).
[44] K. Hummer, J. Harl, and G. Kresse, Phys. Rev. B **80**, 115205 (2009).
[45] G. Nilsson and G. Nelin, Phys. Rev. B **6**, 3777 (1972).
[46] J. Kulda, D. Strauch, P. Pavone, and Y. Ishii, Phys. Rev. B **50**, 13347 (1994).
[47] G. Nilsson and G. Nelin, Phys. Rev. B **3**, 364 (1971).
[48] S. Adachi, *Properties of Group-IV, III-V and II-VI Semiconductors* (Wiley, Chichester, 2005).
[49] M. Cardona, *Light Scattering in Solids II* (Springer, Berlin, 1982).
[50] The free electron-hole space of solutions $|\alpha_e\rangle|\alpha_h\rangle$ is no longer valid if the electron-hole Coulomb interaction is considered. Nevertheless, the main conclusions related to Raman selection rules are valid. The Coulomb interaction will modify the value of the oscillator strength and overlapping integrals $\langle\alpha'_{e,h}|U|\alpha_{e,h}\rangle$.
[51] We denote by X, Y, Z, X', and Y' the [100], [010], [001], [110], and $[1\bar{1}0]$ crystallographic directions with [001] the quantization axis.
[52] In bulk semiconductors this configuration allows the transversal TO phonon, while in NWs a mixture of modes is obtained as a consequence of the reduced symmetry.
[53] Due to symmetry reasons, the contribution of the conduction band at the Γ point is zero.
[54] Ch. Kittel, *Quantum Theory of Solids* (J. Wiley & Sons, New York, 1963).
[55] C. T. Giner and F. Comas, Phys. Rev. B **37**, 4583 (1988).